IEEE Access
Multidisciplinary | Rapid Review | Open Access Journal

Received May 6, 2019, accepted May 26, 2019, date of publication June 6, 2019, date of current version June 20, 2019.

Digital Object Identifier 10.1109/ACCESS.2019.2921240

High-Accuracy Real-Time Monitoring of Heart Rate Variability Using 24 GHz Continuous-Wave Doppler Radar

VLADIMIR L. PETROVI [1], (Student Member, IEEE), MILICA M. JANKOVI [1], (Member, IEEE), ANITA V. LUP I [1,2], VELJKO R. MIHAJLOVI [2], AND JELENA S. POPOVI -BO OVI [1], (Member, IEEE)

[1]School of Electrical Engineering, University of Belgrade, 11120 Belgrade, Serbia
[2]Novelic, 11060 Belgrade, Serbia

Corresponding author: Vladimir L. Petrović (petrovicv@etf.bg.ac.rs)

This work was supported in part by the Innovation Fund of the Republic of Serbia under Grant ID50053, and in part by the Ministry of Education, Science and Technological Development of the Republic of Serbia under Grant OS175016.

ABSTRACT This paper presents a novel algorithm for the estimation of heart rate variability (HRV) features using 24-GHz continuous-wave Doppler radar with quadrature architecture. The proposed algorithm combines frequency and time domain analysis for high-accuracy estimation of beat-to-beat intervals (BBIs). Initially, band pass filtered in-phase (I) and quadrature (Q) radar components are fused into a single combined signal that contains information on the heartbeats. Its frequency domain analysis is used for coarse heart rate estimation. At the same time, the combined signal is processed using a filter bank containing narrowband band pass filters with different center frequencies. One of the band pass filter outputs is selected as the valid output based on the coarse heart rate estimation. Zero crossings in the resulting filter bank output signal represent heartbeats that are used to extract the BBIs. Finally, four HRV features are calculated from the BBIs. The algorithm is tested on real data obtained from recordings on ten human subjects. The mean relative error of extracted BBIs compared to electrocardiogram (ECG) measurement is in the 1.02−2.07 % range. Furthermore, two time-domain and two frequency domain HRV features were calculated from the BBIs. The obtained results show a high level of agreement between radar-extracted and ECG-extracted HRV features. Low computation complexity makes this algorithm suitable for real-time monitoring.

INDEX TERMS Band pass filters, beat-to-beat intervals (BBI), chirp Z-transform, Doppler radar, frequency domain analysis, heart rate variability (HRV), noncontact vital signs monitoring, real-time processing.

I. INTRODUCTION

High-accuracy monitoring of the heart rate variability (HRV) features is required in numerous applications, such as hospital and in-home health care [1], stress and emotions recognition [2], [3], vigilance monitoring [4], anxiety treatments [5], training optimization [6], etc. Real-time monitoring is desirable in most of these applications.

HRV features reflect changes in time intervals between two consecutive heartbeats, the so called beat-to-beat intervals (BBIs). Conventionally, HRV monitoring systems are based on the usage of contact sensors such as ECG (Electrocardiogram) sensors, PPG (Photoplethysmogram) sensors, piezoelectric or piezoresistive sensors [7]. However, the usage of contact sensors has several disadvantages such as limited mobility, discomfort caused by sensors placed on the body and by patients' awareness of the measurement being performed, skin irritation and allergic contact reactions (in the case of infants or sensitive skin in adults), inapplicability on damaged skin (painful skin rashes, burns, hives, etc.), inability to measure through clothes or other obstacles. Non-contact measurements can overcome these problems.

Radar technology is one of the most promising methods for non-contact heart rate measurement [3], [8]–[39]. Based on their hardware architecture, radars used in vital signs detection field are usually classified into the following classes: Continuous-Wave (CW) Doppler radars [8]–[30], Frequency Modulated Continuous Wave (FMCW) radars [3],

The associate editor coordinating the review of this manuscript and approving it for publication was Roberto Gomez-Garcia.

[31]–[34], and Impulse Radio Ultra-Wideband (IR UWB) radars [35]–[38]. IR UWB radars emit short wideband pulses that are reflected from the target back to the receiver. Since the transmitted pulses are wideband, the receiver must be capable for very high-speed operation, especially in short-range applications, like in the vital signs detection where the period between the pulse transmission and the pulse reception is extremely short. Analog-to-digital converter (ADC) used in such applications needs to support high sampling rate. All this leads to high power consumption by the device [30]. Additionally, IR UWB radars are usually not sensitive enough for heartbeat detection [39]. CW and FMCW radars emit sinusoidal electromagnetic wave, reflected from the target, continuously. CW Doppler radars use a single frequency wave modulated by the target's movement, which makes them capable for monitoring relative displacement only. This means that any target's displacement in the radar's field of view (FoV) affects the measurement. Therefore, Doppler radars have difficulties with several simultaneously illuminated targets. On the other hand, FMCW radars can manage both absolute and relative target's displacement detection, based on the frequency and phase difference between the transmitted and reflected chirp signal. As a result, FMCW technology enables detection of vital signs of more than one person [34]. However, FMCW radars have significantly more complex hardware architecture than the simple CW radars, thus they consume more energy from the power supply, and require more complex signal processing methods for the displacement extraction.

The goal of this research was to enable the usage of simple radar architecture and low power compact radar sensor for real-time and fast single person HRV extraction, which is suitable in applications such as health care monitoring, sleep monitoring or drowsiness detection. Even though the CW Doppler radar cannot detect absolute distance, the previous research [8]–[30] shows that the absolute distance information is not necessary in the BBI detection.

A wide range of carrier sine wave frequencies in the CW Doppler radars has been used in the literature. Lower frequency radar systems allow easier extraction of the displacement from the radar signal using the small angle approximation [10]. Higher frequency radar systems have better sensitivity for displacement estimation, which is crucial in the case of small displacements such as chest wall movements caused by heartbeats. Moreover, lower frequency electromagnetic (EM) radiation penetrates the exposed tissue significantly [40], whereas the EM radiation with frequencies higher than 10 GHz is absorbed at skin surface [40], [41].

Various research works have suggested methods for estimation of average heart rate using Doppler radar technology [11], [12], [15], [16], [18], [19], [21], [22]. However, high-accuracy HRV extraction is much more demanding than an average heart rate extraction and requires better estimation of BBIs. The duration of BBIs in a healthy subject changes significantly over time, because of the respiratory sinus arrhythmia [42], emotions of the subject, or their overall physical state [1]–[3], [5], [6]. Therefore, algorithms that accurately detect moments in which heartbeats occur are needed for correct HRV feature estimation.

Recently, the HRV estimation problem has been investigated by several research groups [23]–[29]. Small angle approximation has been applied in [23] for the heartbeat displacement extraction using a 2.4 GHz Doppler radar system. This approach yielded promising results when subjects were in the supine position, but higher error occurred when subjects were sitting still. Moreover, small angle approximation is not suitable for displacement extraction in high frequency radar systems. Wavelet filter bank applied to the demodulated displacement signal has been used in [24]. Filtered displacement signal was further analyzed by the Ensemble Empirical Mode Decomposition (EEMD) for heartbeat extraction. The drawback of the proposed method is the long duration of data acquisition window (15 s) needed for obtaining high-accuracy BBI extraction (2.53−4.83%). Furthermore, the selection of optimal decomposed intrinsic mode functions (IMFs) for heartbeat signal generation is demanding. In several works [25]–[27], HRV features have not been explicitly calculated, but an effort towards fast and accurate heart rate acquisition has been made using the frequency analysis of short time windows, thus enabling further HRV analysis. The time-window-variation techniques combined with the Fast Fourier Transform (FFT) and Wavelet Transform (WT) have been presented in [25] and [26], respectively. Polyphase-basis discrete cosine transform has been used in [27] for the fast heart rate extraction. All three approaches have shown improvements in comparison with the conventional Short-time Fourier Transform (STFT) based techniques, but still have significant error in the heart rate estimation (greater than 3.4%) that would propagate to the HRV features. Heart rate estimation using the frequency-time phase regression (FTPR) technique has been proposed in [28]. This algorithm is very robust in low signal-to-noise ratio (SNR) conditions (lower than 2% error), but uses the long data acquisition window (10 s) as an input for the analysis. This approach can be used in case of low HRV, but it does not apply in general. Spectrogram-based BBI estimation has been presented in [29]. The specific heartbeat signal is created based on the spectrogram of the band pass filtered Doppler radar signal. The created signal has multiple peaks that do not correspond to any heartbeat and must be rejected. Rejection is conducted through adaptive band pass filtering and comprehensive analysis in the time domain. This approach shows an improvement in BBI estimation compared to the previous work, but focuses only on the frequency domain HRV features.

In this paper a novel accurate algorithm for the estimation of HRV features using 24 GHz continuous-wave Doppler radar is presented. The proposed algorithm combines frequency and time domain analysis to accurately estimate BBIs in real-time and to calculate four HRV features. Unlike many other approaches, the proposed method directly uses in-phase and quadrature radar signals for the BBI estimation without

any displacement demodulation techniques, hence providing negligible sensitivity to DC offset and I/Q imbalance. The algorithm is not intensive computationally, which makes it capable for real-time performance, even on platforms with limited hardware resources. Furthermore, the total heartbeat detection delay is small, which is of crucial importance in applications that require fast BBI detection.

Further in this paper, section II describes the theoretical background of the Doppler radar architecture used in the paper and the adopted simulation model of the chest wall displacement caused by heartbeats and breathing. Additionally, simulated Doppler radar signals are analyzed in frequency domain. Section III describes the proposed algorithm for HRV monitoring. Results obtained from the simulated data and data measured in a human subject study are presented and discussed in section IV. Finally, the conclusion is given in section V.

II. THEORETICAL BACKGROUND

A. CONTINUOUS-WAVE DOPPLER RADAR WORKING PRINCIPLE

Continuous-wave (CW) Doppler radar transmits a single frequency sine wave continuously towards a moving target and receives the reflected wave in order to determine the displacement $x(t)$ of the target. The displacement $x(t)$ summarizes all motions that the target makes (respiration, heartbeat and body motions) [22]. In the absence of large-scale body movement, the displacement $x(t)$ originates only from the chest wall displacement due to breathing and heartbeats.

Fig. 1 shows quadrature architecture of the CW Doppler radar system for vital signs monitoring. The carrier sine wave is generated by the local-oscillator (LO) and amplified using a power amplifier (PA). The transmitted signal $T(t)$ is expressed as

$$T(t) = A_T \cos\left(2\pi f t + \theta(t)\right), \tag{1}$$

where A_T and f are the amplitude and the frequency of the transmitted signal, respectively; $\theta(t)$ is the phase noise of the local-oscillator. Since the target is moving, the reflected signal $R(t)$ is the phase-modulated signal expressed as

$$R(t) = A_R \cos\left(2\pi f t - \frac{4\pi d_0}{\lambda} - \frac{4\pi x(t)}{\lambda} + \theta\left(t - \frac{2d_0}{c}\right)\right), \tag{2}$$

where A_R, f and λ are the amplitude, the frequency and the wavelength of the carrier sine wave signal, c is the speed of light, d_0 is the nominal radar-target distance and $x(t)$ is the displacement due to breathing and heartbeats (Fig. 1) [10].

After low-noise amplification (LNA), the receiver demodulates $R(t)$ signal resulting in two baseband signals: in-phase component $b_I(t)$ and quadrature component $b_Q(t)$ expressed as [13]

$$b_I(t) = A_I \cos\left(\theta_0 + \frac{4\pi x(t)}{\lambda} + \Delta\theta(t)\right) + B_I + n_I(t) \tag{3}$$

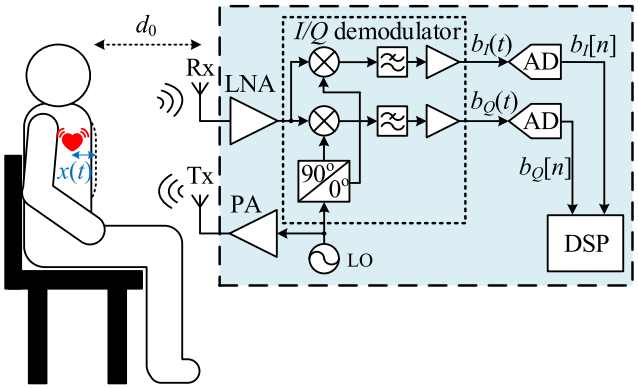

FIGURE 1. Block diagram of the CW Doppler radar measurement system, Tx – transmitting antenna, Rx – receiving antenna.

$$b_Q(t) = A_Q \sin\left(\theta_0 + \frac{4\pi x(t)}{\lambda} + \Delta\theta(t) + \Delta\varphi\right) + B_Q + n_Q(t). \tag{4}$$

In (3) and (4), A_I and A_Q are amplitudes of corresponding I/Q channels ($A_I \neq A_Q$ due to the I/Q amplitude imbalance), B_I and B_Q are DC offsets, θ_0 is the constant phase shift due to reflections from the target surface at d_0 distance, $\Delta\theta(t)$ is the total residual phase noise which can usually be neglected since the distance between target and radar system is small [10]. The phase shift due to I/Q phase imbalance is labeled $\Delta\varphi$. Amplitude noise is represented by $n_I(t)$ and $n_Q(t)$. Quadrature architecture is widely accepted since it does not suffer from the null point issue [10], [13].

After I/Q demodulation, in-phase and quadrature components are sampled using analog-to-digital converters (ADCs). The last Digital Signal Processing (DSP) stage usually includes the following steps: 1) correction of in-phase and quadrature discrete components (removing DC offsets [43], I/Q amplitude and phase imbalance correction [44]), 2) demodulation techniques applied on corrected in-phase and quadrature discrete components for the displacement $x(t)$ extraction (arctangent demodulation [13] or the extended differentiation and cross-multiplication (DACM) demodulation [21]), and 3) estimation of vital signs (respiration rate and heart rate) and their features from the displacement $x(t)$. The first step requires a calibration process and/or real-time correction. The algorithm for HRV feature estimation presented in this paper is applied directly to non-corrected in-phase and quadrature components (expressed in (3) and (4)), which eliminates the need for steps 1) and 2).

B. SIMULATION MODEL OF THE CHEST WALL DISPLACEMENT

The chest wall displacement $x(t)$ was modeled as a sum of the breathing displacement $x_b(t)$ and the much smaller heartbeat displacement $x_h(t)$, neglecting the body movement displacement as in

$$x(t) = x_b(t) + x_h(t). \tag{5}$$

The displacement due to breathing $x_b(t)$ is modeled as per [45], where $x_b(t)$ is the low-pass filtered periodic sequence of quadratic inspiration and exponential expiration waveform $w(t)$, expressed as

$$w(t) = \begin{cases} \dfrac{-K_b}{T_i T_e} t^2 + \dfrac{K_b T}{T_i T_e} t, & t \in [0, T_i] \\ \dfrac{K_b}{1 - e^{-\frac{T_e}{\tau}}} t^2 \left(e^{-\frac{(t-T_e)}{\tau}} - e^{-\frac{T_e}{\tau}} \right), & t \in [T_i, T] \end{cases} \quad (6)$$

where K_b is the model constant used for adjusting the breathing displacement amplitude, T_i is the inspiration time, T_e is the expiration time, and T is the breathing period ($T = T_i + T_e$), whereas τ is the time constant. The physical range of $x_b(t)$ is 4−12 mm, and the physiological breathing rate is 5−25 breaths/min [46].

In the literature, the displacement due to heartbeats $x_h(t)$ has previously been modeled as a sine wave [14], [20], [21], half cycle sine pulses [27], and Gaussian pulse train [28]. Although the heartbeat displacement has a pulsatile nature, its waveform is more complex than the aforementioned waveforms caused by different mechanical behaviors of the heart pump during ventricular depolarization (QRS complex in the ECG) and ventricular repolarization (T wave in the ECG) [47], [48]. Therefore, a single heartbeat displacement $x_{hs}(t)$ is modeled by two distinct pulses as [48]

$$x_{hs}(t) = \eta \cos(\omega t + \gamma \sin(\Omega t)) e^{-\frac{(t-b)^2}{c}}, \quad (7)$$

where b, c, η, ω, γ, and Ω are constant parameters. Total displacement due to heartbeats can be expressed as

$$x_h(t) = \sum_{i=1}^{N_{BBI}} x_{hs} \left(t - \sum_{j=1}^{i} t_{BB}[j] \right), \quad (8)$$

where $t_{BB}[j]$ is the j-th BBI in the BBI sequence. The physical range of the heartbeat displacement amplitude is 0.2−0.5 mm and the physiological heart rate is 45−150 beats/min [49], [50].

Additionally, a respiratory sinus arrhythmia (natural changes in heart rate during a breathing cycle) [42] is also modeled by modulating the BBI sequence with the breathing waveform. The model also includes small changes in the heart rate over a long time interval. In this paper, these changes are modeled as a long period sine wave.

C. FREQUENCY ANALYSIS OF SIMULATED RADAR SIGNALS

In order to analyze the influence of breathing displacement and heartbeat displacement on a spectrum of in-phase and quadrature components, three cases of the chest wall displacements $x(t)$ and corresponding $b_I(t)$ and $b_Q(t)$ signals are simulated: 1) the displacement is only due to breathing ($x(t) = x_b(t)$), 2) the displacement is only due to heartbeats ($x(t) = x_h(t)$), and 3) the displacement is due to both breathing and heartbeats ($x(t) = x_b(t) + x_h(t)$). The discrete form of (3) and (4) is applied to calculate the simulated

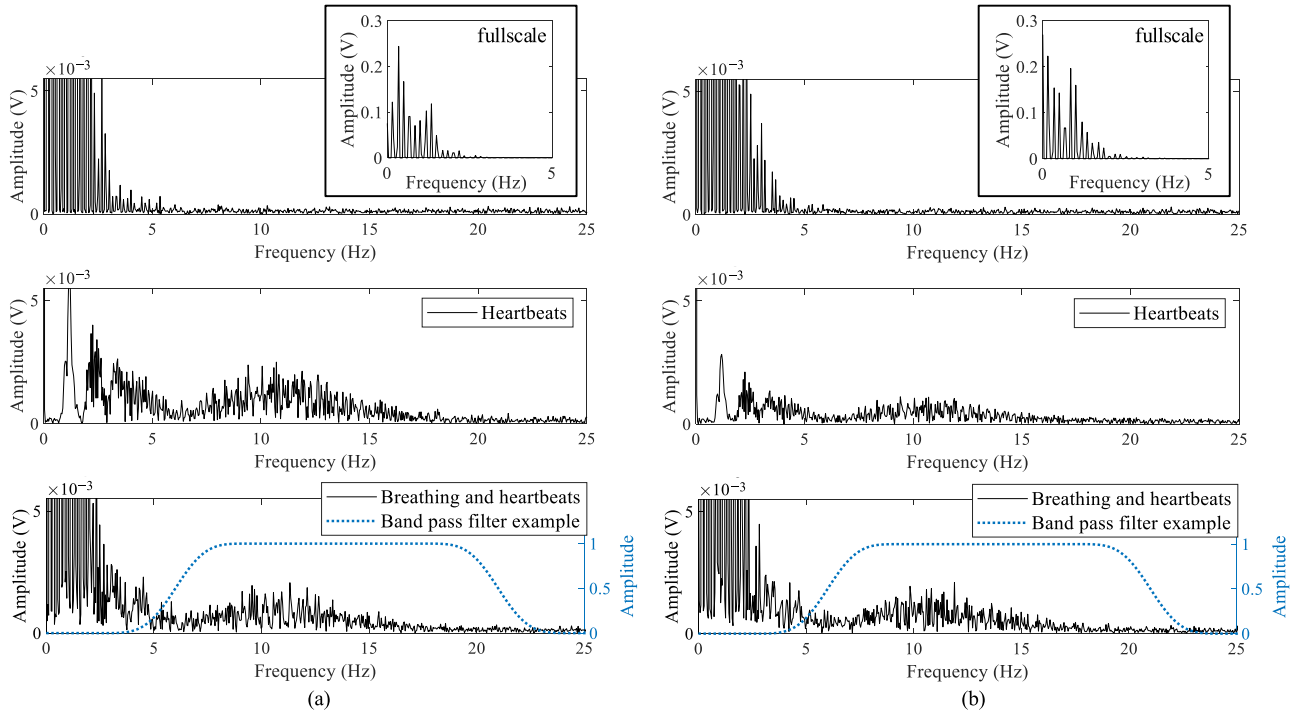

FIGURE 2. Amplitude frequency spectrums of (a) in-phase ($b_I(t)$) and (b) quadrature components ($b_Q(t)$) in three cases of the displacement model: 1) due to breathing only, 2) due to heartbeats only, 3) due to both breathing and heartbeats. An example of the band pass filter for the extraction of heartbeat information is shown by the dashed blue line.

in-phase and quadrature components in all three cases. The simulated carrier frequency is set to 24 GHz. The sampling rate is set to 1 kHz. Frequency analysis of all these sets is performed using the window pre-sum-FFT method [51] in order to reduce spectral leakage. Zoomed frequency spectra for simulated in-phase and quadrature components are shown in Fig. 2(a) and Fig. 2(b), respectively. It can be noticed that there is a part of spectra where higher harmonics of heartbeat frequency components are dominant compared to breathing frequency components. Therefore, application of band pass filtering directly on in-phase and quadrature components can be efficient for attenuating the breathing effects. The amplitude frequency response of one such band pass filter is shown in Fig. 2(a) and Fig. 2(b).

III. METHOD

A. ALGORITHM FOR BBI EXTRACTION

The flowchart of the proposed algorithm for BBI extraction is presented in Fig. 3. Intermediate results of different algorithm stages for the simulated chest wall displacement $x(t)$ defined in section II-B are illustrated in Fig. 4. The first step is the band pass FIR filtering (BPF) of discrete in-phase and quadrature components. This step attenuates low frequency breathing effects and extracts higher heart rate harmonics, as illustrated in section II-C. An example of I and Q channel signals for the simulated chest wall displacement is presented in Fig. 4(b) and corresponding filtered outputs are presented in Fig. 4(c). Instantaneous powers of filtered I and Q signals are summed to represent the influence of both channels (signal p_{IQ} in Fig. 3). The combined instantaneous power is further averaged by applying a moving average filter with a short impulse response (time window) of 0.4 s (signal $p_{MA,\ 0.4}$ in Fig. 3), since the duration of a normal QT segment in the ECG is less than 0.42 s [52]. The amplitude of the resulting $p_{MA,\ 0.4}$ signal varies because of breathing effects, as shown in Fig. 4(d), across different subjects or different radar positions. In order to reduce these variations, a simple Automatic Gain Control (AGC) block is implemented to obtain the normalized power signal (signal p_{norm} in Fig. 3). The normalized power signal is calculated as the ratio of signals $p_{MA,\ 0.4}$ and $p_{MA,\ 1.5}$, where $p_{MA,\ 1.5}$ is the moving averaged combined instantaneous power, obtained by a moving average filter with a longer impulse response of 1.5 s. The example of signal p_{norm} is shown in Fig. 4(e).

The coarse estimation of the heart rate is performed using the chirp Z-transform (CZT) algorithm [53] applied to the autocorrelation of the decimated signal p_{norm}. The signal is decimated by using the anti-aliasing filter and downsampling by a factor of 50 to avoid intensive computing (Fig. 3). The autocorrelation is used in order to highlight the signal's periodicity before the CZT frequency estimation. The data block needed for coarse heart rate estimation should include at least two heartbeats in order to detect any periodicity. Its duration is empirically set to 3.5 s. The coarse estimation can be used for the BBI extraction, but gives unsatisfactory error in HRV feature extraction.

To achieve higher accuracy for BBI estimation, the narrowband band pass filter bank (BP FB) is implemented and applied to the signal p_{norm} (Fig. 3). All filters in the BP FB are designed as FIR band pass filters (BPF_i, $i = 1, 2, \ldots N$) and have the same group delay. Amplitude frequency responses of filters used in the BP FB are shown in Fig. 5. These filters induce the largest group delay in the entire signal processing chain. The stopband attenuation is set to 22 dB in order to obtain the group delay of $\tau_{g,filter\ bank} = 2$ s. However, as shown in Fig. 5, the stopband attenuation rises, which leads to satisfactory weakening of frequency components far from the passband. The algorithm selects one of the BP FB outputs based on the coarse heart rate estimation (band pass filter (BPF) index calculation block in Fig. 3). The filter index is calculated as

$$index = \min\left(\left[\frac{f_{coarse} - f_{offset}}{\Delta f}\right], 1\right), \tag{9}$$

where f_{coarse} is the heart rate frequency calculated in the coarse HR estimator, where f_{offset} is set to 0.9 Hz and Δf is

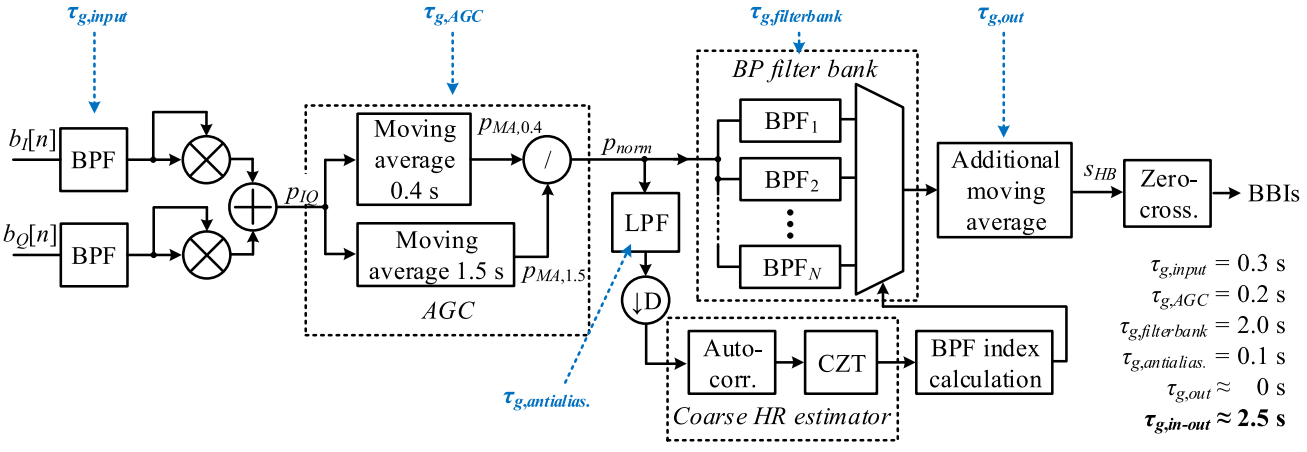

FIGURE 3. Flowchart of the proposed algorithm. AGC – Automatic Gain Control; CZT – Chirp Z-transform.

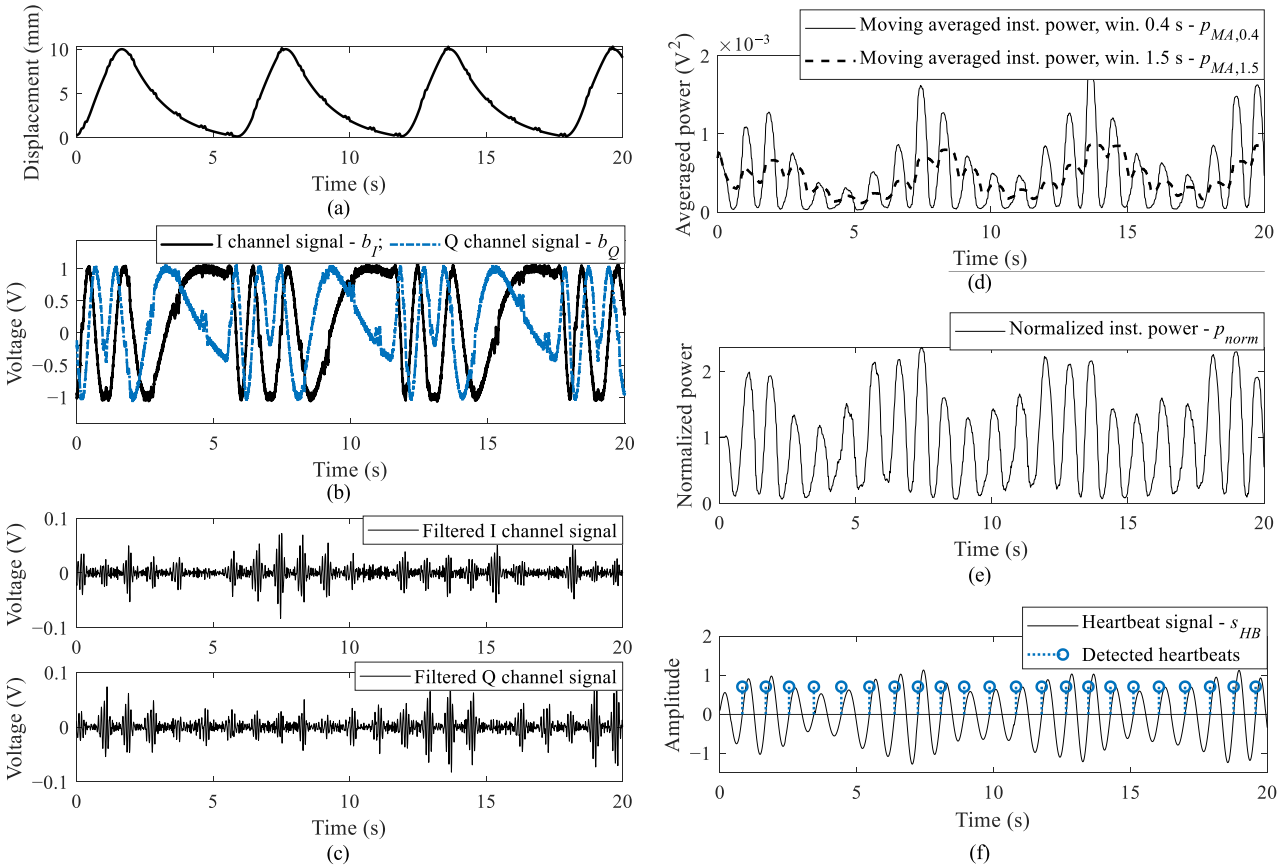

FIGURE 4. Intermediate results of different algorithm stages. (a) Simulated chest wall displacement. (b) Corresponding Doppler radar in-phase and quadrature components for 24 GHz radar (added white Gaussian noise, SNR = 30 dB). (c) Band pass filtered in-phase and quadrature components. (d) Combined instantaneous power of I and Q channels filtered using moving average filter with the time windows of 0.4 s and 1.5 s. (e) Normalized instantaneous power at the output of the AGC block. (f) Extracted heartbeat signal and heartbeats detected at its zero-crossings.

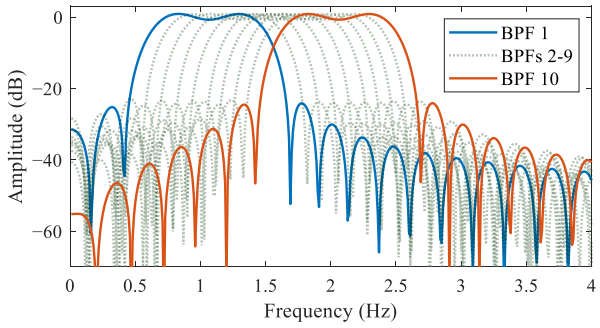

FIGURE 5. Amplitude frequency responses of band pass filters in the band pass filter bank (BP FB).

set to 0.1 Hz (generally, Δf depends on the number of filters in the filter bank).

Small discontinuities may occur when switching from one BP FB output to another. To mitigate these effects, the additional moving average filter is implemented at the BP FB output, producing the so-called heartbeat signal s_{HB}, which can be used for high-accuracy BBI extraction.

Finally, the algorithm detects zero crossings of the heartbeat signal s_{HB} in order to find heartbeat (R wave) positions necessary for BBI calculation (Fig. 4(f)).

Considering previous assumptions, after testing the algorithm performance on the real and simulated data for multiple combinations of algorithm parameters in order to achieve the best performance, the parameters (bandwidths of all band pass filters, moving average filters duration, duration of data block used in the coarse heartrate estimation, parameter f_{offset} in (9) and number of band pass filters in the band pass filter bank) are chosen empirically.

The overall delay of the proposed algorithm, defined as the time from the occurrence of a single heartbeat until its detection, is 2.5 s. It originates mainly from the group delay of filters in the processing chain. Group delays of individual blocks are given in Fig. 3.

The algorithm is not compute-intensive. The duration of processing 180 s of data in MATLAB (MathWorks, USA) using a moderately powerful PC with the Intel Core i5-2320 processor and 8 GB of RAM is only 0.54 s (averaged for 1000 runs). Low computation complexity indicates that the algorithm is suitable for real-time operation.

The advantage of using narrowband BP FB for BBI estimation is illustrated in Fig. 6(a). Simulated BBIs in a 100 s time interval are compared to BBIs extracted using the coarse estimation and BBIs extracted using the BP FB output. BBIs

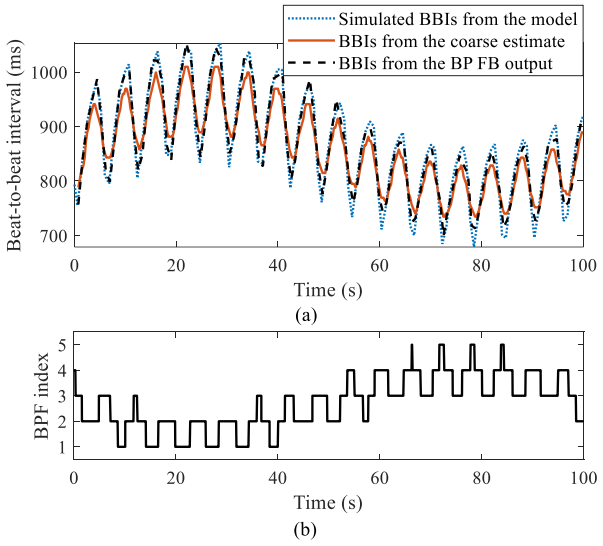

FIGURE 6. (a) Comparison of simulated BBIs, extracted BBIs using coarse estimation and extracted BBIs using narrowband band pass filter bank (BP FB). (b) State changes of band pass filter (BPF) index.

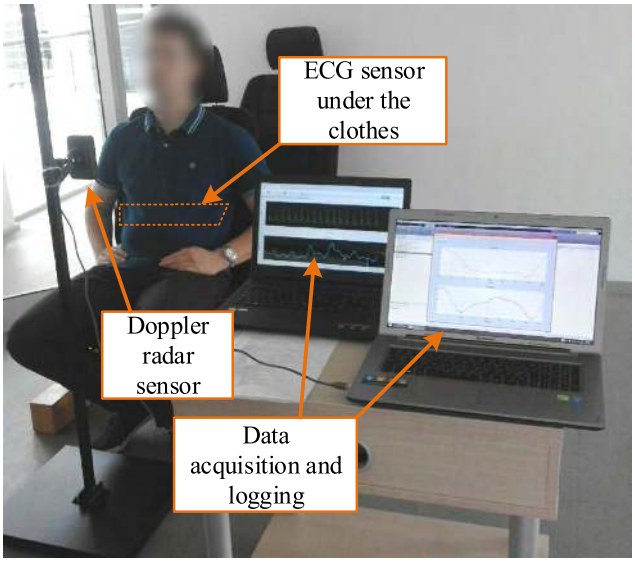

FIGURE 7. Photograph of the experiment setup for measuring HRV features.

are simulated using the model described in section II-B that integrates variability due to respiratory sinus arrhythmia and small variability due to changes of overall physical conditions. The averaging nature of the CZT reduces the ability for detecting all BBI changes. The use of BP FB overcomes this issue and provides a more accurate BBI estimation. Fig. 6(b) shows the changes of the active BPF index corresponding to Fig. 6(a). It can be observed that high-accuracy BBI estimation benefits from multiple band pass filters with different central frequencies.

B. HRV FEATURES

Four HRV features are extracted from the BBIs: standard deviation of BBIs (*SDNN*), the root mean square of successive differences (*RMSSD*), the low frequency power (*LF*), and the high frequency power (*HF*) [54], [55].

SDNN and *RMSSD* are calculated using the following equations

$$SDNN = \sqrt{\frac{1}{N_{BBI}} \sum_{i=1}^{N_{BBI}} \left(t_{BB}[i] - \overline{t_{BB}}\right)^2}, \tag{10}$$

$$RMSSD = \sqrt{\frac{1}{N_{BBI} - 1} \sum_{i=2}^{N_{BBI}} \left(t_{BB}[i] - t_{BB}[i-1]\right)^2}, \tag{11}$$

where N_{BBI} is the number of all detected BBIs and $\overline{t_{BB}}$ is the mean value of all BBIs.

LF and *HF* features are calculated from the power spectral density (PSD) of the BBI sequence by integrating the PSD function within the corresponding frequency band (0.04−0.15 Hz for *LF* and 0.15−0.4 Hz for *HF*). Power spectral density is calculated by using the Fast Fourier Transform (FFT) approach.

C. EXPERIMENT DESIGN AND INSTRUMENTATION DETAILS

The study included ten healthy subjects (seven male and three female, aged 26.1 ± 5.8, with a height of 178.5 ± 10.9 cm and a weight of 71.6 ± 16.3 kg) who did not suffer any cardiac or other chronic disease. All participants have signed informed consent to the study approved by the local ethical committee.

The subjects remained in the sitting position and were breathing normally for 3 min. Two systems were used for data acquisition: the Doppler radar system and Smartex Wearable Wellness System (WWS, Pisa, Italy) as the reference system. Smartex WWS system consists of a belt with ECG and respiration sensors, and a microcontroller that sends data to a remote PC via Bluetooth connection. BBIs are extracted from the ECG using the Pan-Tompkins algorithm [56]. The Doppler radar system was placed in front of the subjects, at a distance of 75 cm, as in Fig. 7.

The compact 24 GHz Doppler radar system Novelic Radar Module NRM24, shown in Fig. 8, was used for measurements presented in this paper. The radar module is commercially available and can be purchased from the Novelic Company, Belgrade. Its dimensions are $8 \times 5 \times 1$ cm. The radar platform contains two stacked printed circuit boards (PCBs): 1) the radar sensor PCB and 2) the acquisition PCB. The radar sensor PCB integrates transceiver and printed transmit (Tx) and receive (Rx) antennas. Antenna radiation pattern is shown in Fig. 9. Elevation and azimuth 3-dB beamwidths are $BW_\theta = 25°$ and $BW_\varphi = 44°$, respectively. The maximum transmitting power at the antenna input is 10 dBm. The radar sensor PCB is plugged into the acquisition PCB. The radar is DC-coupled and baseband in-phase and quadrature signals are filtered at the acquisition PCB using the low pass filter with the cutoff frequency $f_C = 100$ Hz. The acquisition PCB contains an ARM based microcontroller that has a multichannel analog-to-digital converter, which is used for sampling the

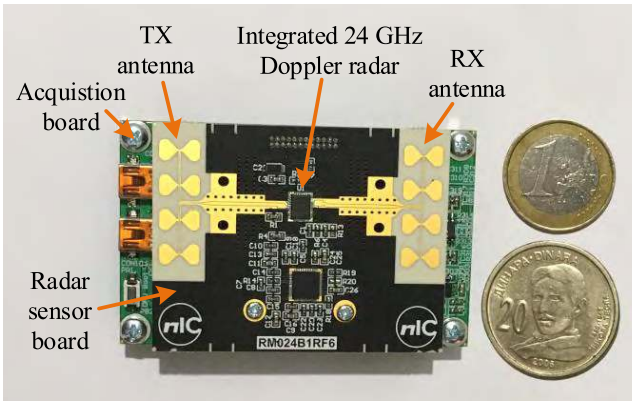

FIGURE 8. 24 GHz Doppler radar system.

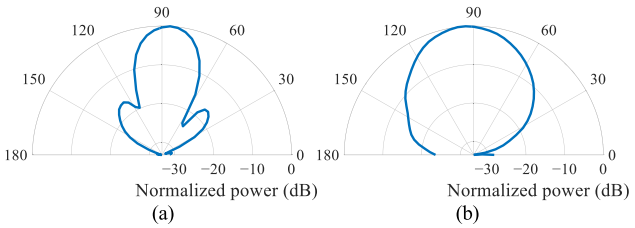

FIGURE 9. Radiation pattern of the radar antenna: (a) elevation plane pattern, (b) azimuth plane pattern.

in-phase and quadrature channel signals. The sampling rate is set to $f_S = 1$ kHz and the acquired data is transmitted to the PC via the serial port. Data logging has been performed using a custom-made application.

Additionally, the radar sensor is characterized by measuring its I/Q imbalance. The I/Q imbalance values are obtained by using a mechanical target described in [57] and an ellipse fit method from [44]. The mechanical target has been adjusted to make enough displacement for producing full ellipse in the in-phase/quadrature plot. The obtained phase imbalance is $\Delta\varphi = 2.91°$, whereas the amplitude imbalance is $A_e = A_Q/A_I = 1.035$.

IV. RESULTS

A. SIMULATED DATA RESULTS

Simulation model, described in section II-B, showed that it is possible to extract heartbeat information directly from in-phase and quadrature signals. Additionally, the model is used for testing the algorithm performance in the presence of noise and I/Q imbalance in several different scenarios. All algorithm parameters in those tests are set to values described in the section III-A.

Fig. 10 shows the influence of noise on algorithm accuracy. This influence is tested for six different simulated breathing rates (BR). The BBI sequence for breathing rate of 8 bpm is shown in Fig. 10(a), as an example. The peak-to-peak amplitude of changes in the BBI sequence, which comes from the simulated respiratory sinus arrhythmia, is set to 150 ms for all BRs. In order to achieve the worst-case scenario

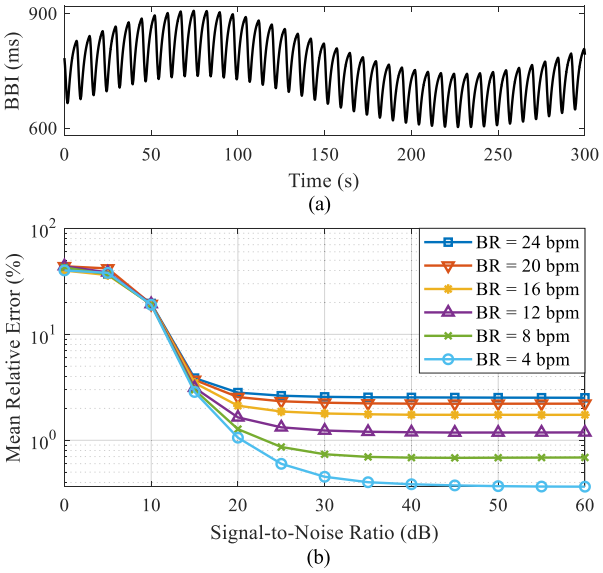

FIGURE 10. (a) Example of the BBI sequence for BR = 8 bpm used for noise influence testing. (b) Mean Relative Error (MRE) of extracted BBIs depending on the SNR at the I and Q signals for different values of breathing rate. $x_{b,max} = 12$ mm, $x_{hs,max} = 0.2$ mm.

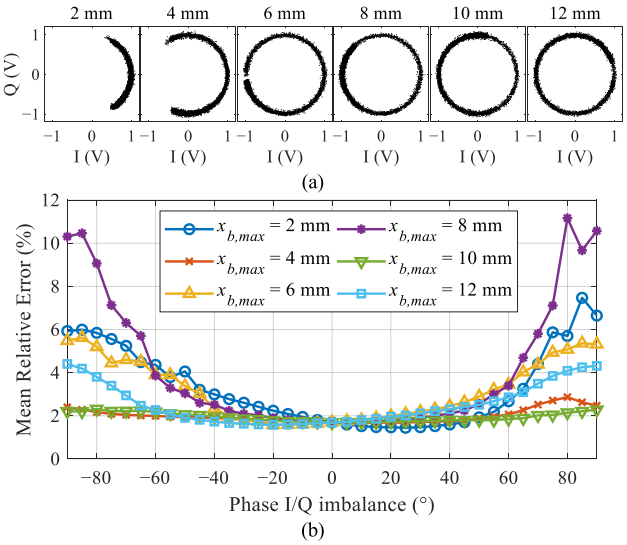

FIGURE 11. (a) I/Q plots for different maximum breathing displacements without I/Q imbalance. (b) Mean Relative Error (MRE) of extracted BBIs depending on the phase I/Q imbalance for different values of maximum breathing displacement. BR = 12 bpm, SNR = 20 dB.

that corresponds to the physical range described in the section II-B, the peak-to-peak amplitude of the breathing displacement is set to maximal 12 mm, whereas the heartbeat displacement is set to minimal 0.2 mm. Fig. 10(b) shows that the minimum SNR needed, for less than 3% mean relative error, is 20 dB. The mean relative error is larger for larger values of the breathing rate, which can be explained by good coarse estimation of lower heartrates capacity that further influence the total error performance.

The amplitude I/Q imbalance does not affect the algorithm performance since no displacement demodulation

technique is used. However, when the phase I/Q imbalance is large, it can affect the algorithm error performance. Fig. 11(a) shows that full ellipse is not present in the in-phase/quadrature (I/Q) plot in the case of displacements that are lower than 6.25 mm (for 24 GHz radar). Because of this, the influence of the I/Q imbalance is tested for different breathing displacements. The SNR is set to 20 dB which is the critical value obtained in the noise influence analysis. The error performance is shown in Fig. 11(b). It can be noticed that the phase I/Q imbalance affect error performance at large values of $\Delta\varphi$ parameter. However, the analysis shows that the influence on the error performance is low in the $\Delta\varphi$ range of $-40°$ to $40°$, which is more than enough for most available Doppler radars.

The algorithm is not sensitive to DC offsets or small changes in I/Q plane center position [43], since both in-phase and quadrature signal components are filtered by using the input band pass filter.

B. MEASURED DATA RESULTS

Fig. 12 shows a 20 s sample of time-aligned ECG signal obtained by the Smartex WWS and the extracted heartbeat signal obtained from the Doppler radar data. Zero-crossings detected by the proposed algorithm correspond well with the R peaks in the ECG.

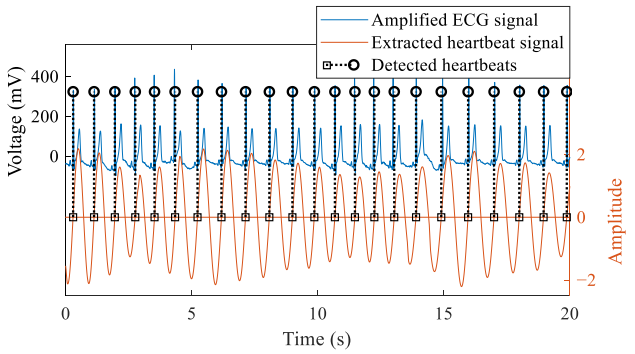

FIGURE 12. The 20 s sample of time-aligned ECG (R peaks are marked by circles) and estimated heartbeat signal s_{HB} from the Doppler radar data (zero-crossing detections are marked by squares).

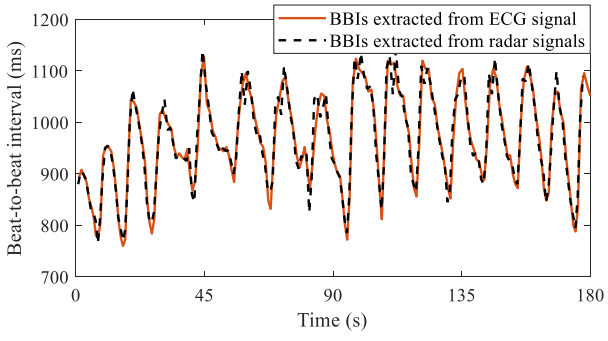

FIGURE 13. 180 s sample of BBIs extracted from the reference ECG signal and from the Doppler radar signal using the proposed algorithm.

Fig. 13 shows the high agreement between BBI time diagrams extracted from the reference ECG signal and from the Doppler radar data for one subject over the whole 3 min acquisition interval.

Previous investigations in this field have used different approaches for error calculation. In order to compare results of the proposed algorithm with the literature, three different ways for error calculation are implemented:

- The root-mean-squared error (*RMSE*) is expressed as

$$RMSE = \sqrt{\frac{1}{N_{BBI}} \sum_{i=1}^{N_{BBI}} \left(t_{BB,radar}[i] - t_{BB,ECG}[i]\right)^2}. \quad (12)$$

- The root-mean-squared relative error (*RMSRE*) is calculated as the root-mean-squared error (*RMSE*) divided by the mean value of reference BBIs as

$$RMSRE = \frac{\sqrt{\frac{1}{N_{BBI}} \sum_{i=1}^{N_{BBI}} \left(t_{BB,radar}[i] - t_{BB,ECG}[i]\right)^2}}{\frac{1}{N_{BBI}} \sum_{i=1}^{N_{BBI}} t_{BB,ECG}[i]}. \quad (13)$$

- Mean relative error (*MRE*) is expressed as

$$MRE = \frac{1}{N_{BBI}} \sum_{i=1}^{N_{BBI}} \frac{\left|t_{BB,radar}[i] - t_{BB,ECG}[i]\right|}{t_{BB,ECG}[i]}. \quad (14)$$

In (12), (13), and (14), N_{BBI} is the number of detected BBIs, $t_{BB,radar}$ is the BBI extracted from the Doppler radar signal, and $t_{BB,ECG}$ is the BBI extracted from the ECG signal.

Table 1 shows the results of BBI extraction for both approaches presented in section III: the CZT based BBI extraction, used for coarse BBI estimates, and the BP FB based approach. The algorithm parameters are the same for all test subjects. Results are compared with those obtained from the reference ECG signal. The mean relative errors for CZT and BP FB approaches are 1.83−5.21 % and 1.02−2.07 %, respectively. The error is lower when BP FB is used for all subjects.

Additionally, the Bland-Altman analysis [58] is performed for assessing the agreement between the BBIs extracted from radar signals and from the ECG signal. Table 1 compares biases and limits of agreement for all subjects. The bias is the average of all differences between the BBIs extracted from the Doppler radar signals and the BBIs estimated from ECG signals. Limits of agreement are defined by the 95 % confidence interval. The lower limit of agreement and the upper limit of agreement are defined as

$$LLoA = Bias - 2SD, \quad (15)$$

$$ULoA = Bias + 2SD, \quad (16)$$

where the *SD* is the standard deviation of all differences. The analysis shows high agreement between radar-based and ECG-based BBIs for subjects with exceedingly various average heart rates (48.2−88.1 bpm), which makes this testing more reliable.

TABLE 1. Results of extracted beat-to-beat intervals for 10 subjects.

Subject	BBIs average (ms)			*RMSRE* (%)		*MRE* (%)		Bland Altman Analysis (ms)					
	ECG	Radar		CZT	BP FB	CZT	BP FB	CZT			BP FB		
		CZT	BP FB					*Bias*	*LLoA*	*ULoA*	*Bias*	*LLoA*	*ULoA*
1	713.5	709.3	714.7	2.28	**1.32**	1.83	**1.03**	−6.44	−36.21	23.33	**0.23**	**−18.22**	**18.69**
2	1244.2	1222.1	1240.6	6.56	**2.70**	5.21	**2.07**	−29.92	−176.05	116.21	**−0.52**	**−64.57**	**63.53**
3	812.7	803.4	811.2	2.36	**1.31**	1.98	**1.02**	−8.28	−42.53	25.98	**0.05**	**−20.83**	**20.93**
4	842.7	831.8	841.4	4.70	**2.68**	3.73	**2.03**	−12.26	−86.96	62.44	**−0.11**	**−44.49**	**44.28**
5	820.6	811.9	821.2	2.99	**1.98**	2.40	**1.51**	−11.33	−53.76	31.09	**−0.04**	**−31.52**	**31.44**
6	832.7	824.9	832.2	3.46	**2.08**	2.87	**1.68**	−8.48	−63.35	46.39	**0.39**	**−33.84**	**34.62**
7	961.5	955.7	960.5	4.00	**1.41**	2.84	**1.08**	−12.13	−84.45	60.19	**0.13**	**−27.55**	**27.81**
8	799.3	805.5	805.5	3.09	**1.94**	2.50	**1.55**	−9.67	−54.46	35.12	**0.08**	**−31.26**	**31.42**
9	679.4	676.3	679.2	4.50	**1.89**	2.61	**1.50**	−4.38	−93.70	84.94	**0.05**	**−24.86**	**24.97**
10	763.1	758.0	763.3	4.38	**2.37**	3.51	**1.72**	−9.75	−72.70	53.21	**−0.74**	**−35.32**	**33.83**

TABLE 2. Results of extracted heart rate variability features for 10 subjects.

Subject	*SDNN* (ms)			*RMSSD* (ms)			*LF* (ms^2)			*HF* (ms^2)		
	ECG	Radar		ECG	Radar		ECG	Radar		ECG	Radar	
		CZT	BP FB		CZT	BP FB		CZT	BP FB		CZT	BP FB
1	35.3	34.0	35.1	17.6	48.2	18.9	401.9	351.8	380.4	43.3	32.8	54.2
2	109.2	89.8	113.4	100.3	143.7	106.0	2170.1	1816.6	2123.3	1667.2	965.4	1734.3
3	31.7	22.3	28.5	29.6	24.7	24.7	123.5	98.9	122.1	172.7	41.5	107.0
4	61.5	36.9	60.8	52.3	54.3	54.5	908.7	666.3	846.3	497.4	207.6	500.0
5	45.9	40.3	44.9	32.0	40.9	31.1	315.3	262.4	316.3	175.9	37.7	130.9
6	41.5	25.9	44.6	38.7	31.6	42.8	234.4	187.3	240.3	283.0	124.4	387.5
7	92.2	72.5	90.3	56.6	117.1	56.8	2586.2	2165.4	2494.1	547.9	247.0	513.9
8	41.9	33.1	42.9	32.3	33.2	36.9	201.5	160.0	201.6	241.5	97.3	279.1
9	38.8	37.6	39.4	20.6	40.4	25.1	255.5	305.1	239.3	111.3	357.0	118.9
10	62.9	46.0	59.1	44.1	73.5	44.3	706.7	540.7	616.4	1077.0	620.1	903.3

Table 2 shows the calculated heart rate variability (HRV) features based on the BBIs extracted from the Doppler radar signals and from ECG signals. Fig. 14 shows the bar chart of calculated *SDNN*, *RMSSD*, *LF* and *HF* HRV features, and also the *LnLF* and the *LnHF* parameters, calculated as the natural logarithm of *LF* and *HF* normalized to 1 ms^2, which can be used in some applications as well [55]. Results show high agreement between HRV features obtained from ECG and Doppler radar signals in the case of the BP FB approach for BBI extraction. CZT based HRV extraction yields less accurate results than the extraction from the BP FB output signal, especially for the HF parameter. This confirms the significance of the BP FB in the processing chain, even if that is not clearly evident from the results in Table 1. It is also important to notice that test subjects have various HRV features within a wide range of typical values for healthy adults [59], which once again confirms the reliability of the testing.

In Table 3, results of the proposed algorithm are compared to the results from relevant previously published papers that dealt with HRV measurements and short time window heart rate determination. The approach presented in this paper has a lower error than any other considered method with similar duration of the time window.

V. CONCLUSION

In this paper, a novel method for the extraction of HRV features using the Doppler radar technology is presented. The proposed method is capable for real-time applications and provides a small delay from the occurrence of the heartbeat until its detection ($\sim$ 2.5 s). It uses the frequency domain analysis for coarse estimation of the heart rate frequency and the narrowband band pass filtering for further refinement. Moreover, the algorithm is virtually insensitive to the I/Q imbalance, since it does not use any demodulation technique for displacement extraction.

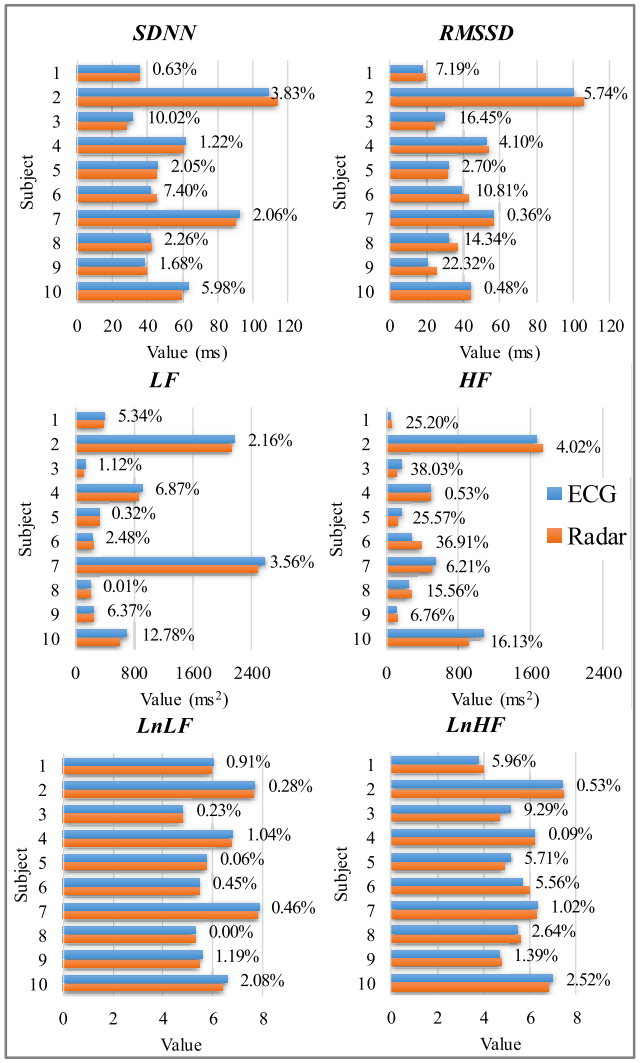

FIGURE 14. Bar chart of calculated ECG based and radar based HRV features and relative error for all subjects.

TABLE 3. Comparison of beat-to-beat intervals detection accuracy between the proposed method and the previous work.

	Radar freq. (GHz)	N_{SUB}	T_{MEAS} (s)	T_W (s)	Avg. *RMSRE* (%)	Avg. *MRE* (%)	Avg. *RMSE* (ms)
[24]	5.8	10	240	15	**3.67**	-	-
[25]	5.8	4	30	2–5	-	**3.37**	-
[26]	5.8	4	60	3–5	-	**3.52**	-
[29]	24	10	120	2–3	-	-	**47.5**
This work	24	10	180	3.5	**1.97**	**1.54**	**16.7**

N_{SUB}: number of subjects; T_{MEAS}: total measurement time for each subject; T_W: observation window duration; Avg.: averaged; -: not available.

The method has been validated on a group of ten subjects with a wide range of heart rates. Multiple error metrics and Bland-Altman analysis have shown a high level of agreement between BBIs extracted from the Doppler radar signals and from the reference ECG signals. The mean relative error for the coarse estimation of BBIs in the frequency domain was less than 5.21 %, but with the addition of the band pass filter bank for BBI extraction refinement, the mean relative error became lower than 2.07 % for all tested subjects. The obtained results show that the proposed method outperforms all of the previously published methods considered herein that dealt with the HRV extraction and heart rate extraction in short time intervals. High-accuracy BBI extraction enables high-accuracy estimation of two time-domain (*SDNN*, *RMSSD*) and two frequency-domain (*LF*, *HF*) HRV features.

In future, the plan is to design radar antennas with higher directivity and use them for radars with even higher frequencies than 24 GHz in order to obtain better results. Higher directivity antennas would detect fewer random body movements, thus providing better error performance. Moreover, the radar system with even higher carrier frequency would be more sensitive to small chest displacements such as heartbeat displacement. If so, the system should be able to detect BBIs and HRV features even more accurately.

ACKNOWLEDGMENT

Authors are thankful to Prof. Jelena Ćertić and Prof. Lazar Saranovac from the University of Belgrade – School of Electrical Engineering, Belgrade, Serbia, Mr. Dejan Rakić, M.Sc. E. E., from Novelic, Belgrade, Serbia, and Nebojša Malešević, Ph.D., Postdoctoral fellow at Lund University, Lund, Sweden, for valuable comments and discussions.

REFERENCES

[1] A. T. Mazzeo, E. L. Monaca, R. Di Leo, F. Vita, and L. B. Santamaria, "Heart rate variability: A diagnostic and prognostic tool in anesthesia and intensive care," *Acta Anaesthesiol. Scand.*, vol. 55, no. 7, pp. 797–811, Aug. 2011.

[2] J. A. Healey and R. W. Picard, "Detecting stress during real-world driving tasks using physiological sensors," *IEEE Trans. Intell. Transp. Syst.*, vol. 6, no. 2, pp. 156–166, Jun. 2005.

[3] M. Zhao, F. Adib, and D. Katabi, "Emotion recognition using wireless signals," in *Proc. 22nd Annu. Int. Conf. Mobile Comput. Netw.*, New York, NY, USA, Oct. 2016, pp. 95–108.

[4] B.-G. Lee, B.-L. Lee, and W.-Y. Chung, "Wristband-type driver vigilance monitoring system using smartwatch," *IEEE Sensors J.*, vol. 15, no. 10, pp. 5624–5633, Oct. 2015.

[5] J. A. Chalmers, D. S. Quintana, M. J.-A. Abbott, and A. H. Kemp, "Anxiety disorders are associated with reduced heart rate variability: A meta-analysis," *Frontiers Psychiatry*, vol. 5, Jul. 2014, Art. no. 80.

[6] J. Morales, J. M. Álamo, X. García-Massó, J. L. López, P. Serra-Añó, and L.-M. González, "Use of heart rate variability in monitoring stress and recovery in judo athletes," *J. Strength Conditioning Res.*, vol. 28, no. 7, pp. 1896–1905, Jul. 2014.

[7] J. G. Webster, *Medical Instrumentation: Application and Design*, 4th ed. New York, NY, USA: Wiley, 2009.

[8] A. Droitcour, V. Lubecke, J. Lin, and O. Boric-Lubecke, "A microwave radio for Doppler radar sensing of vital signs," in *IEEE MTT-S Int. Microw. Symp. Dig.*, vol. 1, May 2001, pp. 175–178.

[9] O. B. Lubecke, P.-W. Ong, and V. M. Lubecke, "10 GHz Doppler radar sensing of respiration and heart movement," in *Proc. IEEE 28th Annu. Northeast Bioeng. Conf.*, Philadelphia, PA, USA, Apr. 2002, pp. 55–56.

[10] A. D. Droitcour, O. Boric-Lubecke, V. M. Lubecke, J. Lin, and G. T. A. Kovacs, "Range correlation and I/Q performance benefits in single-chip silicon Doppler radars for noncontact cardiopulmonary monitoring," *IEEE Trans. Microw. Theory Techn.*, vol. 52, no. 3, pp. 838–848, Mar. 2004.

[11] Y. Xiao, J. Lin, O. Boric-Lubecke, and V. M. Lubecke, "Frequency-tuning technique for remote detection of heartbeat and respiration using low-power double-sideband transmission in the Ka-band," *IEEE Trans. Microw. Theory Techn.*, vol. 54, no. 5, pp. 2023–2032, May 2006.

[12] C. Li, Y. Xiao, and J. Lin, "Experiment and spectral analysis of a low-power Ka-band heartbeat detector measuring from four sides of a human body," *IEEE Trans. Microw. Theory Techn.*, vol. 54, no. 12, pp. 4464–4471, Dec. 2006.

[13] B.-K. Park, O. Boric-Lubecke, and V. M. Lubecke, "Arctangent demodulation with DC offset compensation in quadrature Doppler radar receiver systems," *IEEE Trans. Microw. Theory Techn.*, vol. 55, no. 5, pp. 1073–1079, May 2007.

[14] C. Li and J. Lin, "Random body movement cancellation in Doppler radar vital sign detection," *IEEE Trans. Microw. Theory Techn.*, vol. 56, no. 12, pp. 3143–3152, Dec. 2008.

[15] J. H. Choi and D. K. Kim, "A remote compact sensor for the real-time monitoring of human heartbeat and respiration rate," *IEEE Trans. Biomed. Circuits Syst.*, vol. 3, no. 3, pp. 181–188, Jun. 2009.

[16] C. Li, J. Ling, J. Li, and J. Lin, "Accurate Doppler radar noncontact vital sign detection using the RELAX algorithm," *IEEE Trans. Instrum. Meas.*, vol. 59, no. 3, pp. 687–695, Mar. 2010.

[17] F.-K. Wang, T.-S. Horng, K.-C. Peng, J.-K. Jau, J.-Y. Li, and C.-C. Chen, "Single-antenna Doppler radars using self and mutual injection locking for vital sign detection with random body movement cancellation," *IEEE Trans. Microw. Theory Techn.*, vol. 59, no. 12, pp. 3577–3587, Dec. 2011.

[18] S. Bakhtiari, S. Liao, T. Elmer, N. S. Gopalsami, and A. C. Raptis, "A real-time heart rate analysis for a remote millimeter wave I-Q sensor," *IEEE Trans. Biomed. Eng.*, vol. 58, no. 6, pp. 1839–1845, Jun. 2011.

[19] P. Bechet, R. Mitran, and M. Munteanu, "A non-contact method based on multiple signal classification algorithm to reduce the measurement time for accurately heart rate detection," *Rev. Sci. Instrum.*, vol. 84, no. 8, Aug. 2013, Art. no. 084707.

[20] C. Li, V. M. Lubecke, O. Boric-Lubecke, and J. Lin, "A review on recent advances in Doppler radar sensors for noncontact healthcare monitoring," *IEEE Trans. Microw. Theory Techn.*, vol. 61, no. 5, pp. 2046–2060, May 2013.

[21] J. Wang, X. Wang, L. Chen, J. Huangfu, C. Li, and L. Ran, "Noncontact distance and amplitude-independent vibration measurement based on an extended DACM algorithm," *IEEE Trans. Instrum. Meas.*, vol. 63, no. 1, pp. 145–153, Jan. 2014.

[22] Q. Lv, L. Chen, K. An, J. Wang, H. Li, D. Ye, J. Huangfu, C. Li, and L. Ran, "Doppler vital signs detection in the presence of large-scale random body movements," *IEEE Trans. Microw. Theory Techn.*, vol. 66, no. 9, pp. 4261–4270, Sep. 2018.

[23] W. Massagram, V. M. Lubecke, A. Høst-Madsen, and O. Boric-Lubecke, "Assessment of heart rate variability and respiratory sinus arrhythmia via Doppler radar," *IEEE Trans. Microw. Theory Techn.*, vol. 57, no. 10, pp. 2542–2549, Oct. 2009.

[24] W. Hu, Z. Zhao, Y. Wang, H. Zhang, and F. Lin, "Noncontact accurate measurement of cardiopulmonary activity using a compact quadrature Doppler radar sensor," *IEEE Trans. Biomed. Eng.*, vol. 61, no. 3, pp. 725–735, Mar. 2014.

[25] J. Tu and J. Lin, "Fast acquisition of heart rate in noncontact vital sign radar measurement using time-window-variation technique," *IEEE Trans. Instrum. Meas.*, vol. 65, no. 1, pp. 112–122, Jan. 2016.

[26] M. Li and J. Lin, "Wavelet-transform-based data-length-variation technique for fast heart rate detection using 5.8-GHz CW Doppler radar," *IEEE Trans. Microw. Theory Techn.*, vol. 66, no. 1, pp. 568–576, Jan. 2018.

[27] J. Park, J. W. Ham, S. Park, D. H. Kim, S. J. Park, H. Kang, and S. O. Park, "Polyphase-basis discrete cosine transform for real-time measurement of heart rate with CW Doppler radar," *IEEE Trans. Microw. Theory Techn.*, vol. 66, no. 3, pp. 1644–1659, Mar. 2018.

[28] M. Nosrati and N. Tavassolian, "High-accuracy heart rate variability monitoring using Doppler radar based on Gaussian pulse train modeling and FTPR algorithm," *IEEE Trans. Microw. Theory Techn.*, vol. 66, no. 1, pp. 556–567, Jan. 2018.

[29] K. Yamamoto, K. Toyoda, and T. Ohtsuki, "Spectrogram-based non-contact RRI estimation by accurate peak detection algorithm," *IEEE Access*, vol. 6, pp. 60369–60379, Oct. 2018.

[30] C. Gu, "Short-range noncontact sensors for healthcare and other emerging applications: A review," *Sensors*, vol. 16, no. 8, p. 1169, Aug. 2016.

[31] G. Wang, J.-M. Muñoz-Ferreras, C. Gu, C. Li, and R. Gómez-García, "Application of linear-frequency-modulated continuous-wave (LFMCW) radars for tracking of vital signs," *IEEE Trans. Microw. Theory Techn.*, vol. 62, no. 6, pp. 1387–1399, Jun. 2014.

[32] S. Wang, A. Pohl, T. Jaeschke, M. Czaplik, M. Kony, S. Leonhardt, and N. Pohl, "A novel ultra-wideband 80 GHz FMCW radar system for contactless monitoring of vital signs," in *Proc. IEEE 37th Annu. Int. Conf. Eng. Med. Biol. Soc.*, Milan, Italy, Aug. 2015, pp. 4978–4981.

[33] M. He, Y. Nian, and Y. Gong, "Novel signal processing method for vital sign monitoring using FMCW radar," *Biomed. Signal Process. Control*, vol. 33, pp. 335–345, Mar. 2017.

[34] A. Ahmad, J. C. Roh, D. Wang, and A. Dubey, "Vital signs monitoring of multiple people using a FMCW millimeter-wave sensor," in *Proc. IEEE Radar Conf.*, Oklahoma City, OK, USA, Apr. 2018, pp. 1450–1455.

[35] F. Khan and S. H. Cho, "A detailed algorithm for vital sign monitoring of a stationary/non-stationary human through IR-UWB radar," *Sensors*, vol. 17, no. 2, p. 290, 2017.

[36] W. P. Huang, C. H. Chang, and T. H. Lee, "Real-time and noncontact impulse radio radar system for μm movement accuracy and vital-sign monitoring applications," *IEEE Sensors J.*, vol. 17, no. 8, pp. 2349–2358, Apr. 2017.

[37] E. Schires, P. Georgiou, and T. S. Lande, "Vital sign monitoring through the back using an UWB impulse radar with body coupled antennas," *IEEE Trans. Biomed. Circuits Syst.*, vol. 12, no. 2, pp. 292–302, Mar. 2018.

[38] Y. Lee, J. Y. Park, Y. W. Choi, H. K. Park, S. H. Cho, S. H. Cho, and Y. H. Lim, "A novel non-contact heart rate monitor using impulse-radio ultra-wideband (IR-UWB) radar technology," *Sci. Rep.*, vol. 8, Aug. 2018, Art. no. 13053.

[39] T. Sakamoto, R. Imasaka, H. Taki, T. Sato, M. Yoshioka, K. Inoue, T. Fukuda, and H. Sakai, "Feature-based correlation and topological similarity for interbeat interval estimation using ultrawideband radar," *IEEE Trans. Biomed. Eng.*, vol. 63, no. 4, pp. 747–757, Apr. 2016.

[40] S. Gabriely, R. Lau, and C. Gabriel, "The dielectric properties of biological tissues: II. Measurements in the frequency range 10 Hz to 20 GHz," *Phys. Med. Biol.*, vol. 41, no. 11, pp. 2251–2269, 1996.

[41] *Electromagnetic Fields and Public Health: Radars and Human Health*, World Health Org., Geneva, Switzerland, 1999. Accessed: Dec. 9, 2018. [Online]. Available: https://www.who.int/peh-emf/publications/facts/fs226/en

[42] J. A. Hirsch and B. Bishop, "Respiratory sinus arrhythmia in humans: How breathing pattern modulates heart rate," *Amer. J. Physiol.-Heart Circulat. Physiol.*, vol. 241, no. 4, pp. H620–629, Oct. 1981.

[43] M. Zakrzewski, H. Raittinen, and J. Vanhala, "Comparison of center estimation algorithms for heart and respiration monitoring with microwave Doppler radar," *IEEE Sensors J.*, vol. 12, no. 3, pp. 627–634, Mar. 2012.

[44] A. Singh, X. Gao, E. Yavari, M. Zakrzewski, X. H. Cao, V. Lubecke, and O. Boric-Lubecke, "Data-based quadrature imbalance compensation for a CW Doppler radar system," *IEEE Trans. Microw. Theory Techn.*, vol. 61, no. 4, pp. 1718–1724, Apr. 2013.

[45] A. Albanese, L. Cheng, M. Ursino, and N. W. Chbat, "An integrated mathematical model of the human cardiopulmonary system: Model development," *Amer. J. Physiol. Heart Circulat. Physiol.*, vol. 310, no. 7, pp. H899–H921, Apr. 2016.

[46] A. De Groote, M. Wantier, G. Cheron, M. Estenne, and M. Paiva, "Chest wall motion during tidal breathing," *J. Appl. Physiol.*, vol. 83, pp. 1531–1537, Nov. 1997.

[47] C. Yang and N. Tavassolian, "Motion artifact cancellation of seismocardiographic recording from moving subjects," *IEEE Sensors J.*, vol. 16, no. 14, pp. 5702–5708, Jul. 2016.

[48] M. Nosrati and N. Tavassolian, "Accurate Doppler radar-based cardiopulmonary sensing using chest-wall acceleration," *IEEE J. Electromagn., RF Microw. Med. Biol.*, vol. 3, no. 1, pp. 41–47, Mar. 2019.

[49] G. Ramachandran and M. Singh, "Three-dimensional reconstruction of cardiac displacement patterns on the chest wall during the P, QRS and T-segments of the ECG by laser speckle inteferometry," *Med. Biol. Eng. Comput.*, vol. 27, no. 5, pp. 525–530, Sep. 1989.

[50] G. Shafiq and G. K. C. Veluvolu, "Surface chest motion decomposition for cardiovascular monitoring," *Sci. Rep.*, vol. 4, May 2014, Art. no. 5093.

[51] R. G. Lyons, "A practical spectrum analyzer," in *Understanding Digital Signal Processing*, 2nd ed. Upper Saddle River, NJ, USA: Prentice-Hall, 2004, pp. 544–547.

[52] C. Saritha, V. Sukanya, and Y. N. Murthy, "ECG signal analysis using wavelet transforms," *Bulg. J. Phys.*, vol. 35, no. 1, pp. 68–77, Feb. 2008.

[53] L. Rabiner, R. W. Schafer, and C. Rader, "The chirp Z-transform algorithm," *IEEE Trans. Audio Electroacoust.*, vol. AU-17, no. 2, pp. 86–92, Jun. 1961.
[54] H. M. Wang and S. C. Huang, "SDNN/RMSSD as a surrogate for LF/HF: A revised investigation," *Model. Simul. Eng.*, vol. 2012, pp. 931943-1–931943-8, Jun. 2012.
[55] F. Shaffer and J. P. Ginsberg, "An overview of heart rate variability metrics and norms," *Frontiers Public Health*, vol. 5, Sep. 2017, Art. no. 258.
[56] J. Pan and W. J. Tompkins, "A real-time QRS detection algorithm," *IEEE Trans. Biomed. Eng.*, vol. BME-32, no. 3, pp. 230–236, Mar. 1985.
[57] V. Petrović, N. Malešević, M. Janković, B. Petrović, and V. Mihajlović, "System for validation of Doppler radar sensors for heartbeat and respiration monitoring," in *Proc. 4th Int. Conf. Elect., Electron. Comput. Eng.*, Zlatibor, Serbia, Jun. 2017, pp. 1–5, Paper BTI1.6.
[58] J. M. Bland and D. G. Altman, "Statistical methods for assessing agreement between two methods of clinical measurement," *Lancet*, vol. 1, pp. 307–310, Feb. 1986.
[59] D. Nunan, G. R. Sandercock, and D. A. Brodie, "A quantitative systematic review of normal values for short-term heart rate variability in healthy adults," *Pacing Clin. Electrophysiol.*, vol. 33, no. 11, pp. 1407–1417, Nov. 2010.

VLADIMIR L. PETROVI (S'19) received the B.Sc. and M.Sc. degrees in electrical engineering from the School of Electrical Engineering, University of Belgrade, Belgrade, Serbia, in 2014 and 2015, respectively.

He is currently a Teaching and Research Assistant with the School of Electrical Engineering, University of Belgrade, Serbia, where he is currently pursuing the Ph.D. degree. His research interests include biomedical signal and image processing, VLSI design, communication systems architectures, and hardware implementations of signal processing algorithms.

Mr. Petrović is a Student Member of the IEEE Signal Processing Society. He was a recepient of the Best Young Researcher's Paper Award at IcETRAN 2016, Serbia.

MILICA M. JANKOVI (M'11) received B.Sc., M.Sc., and Ph.D. degrees in electrical engineering from the School of Electrical Engineering, University of Belgrade, Belgrade, Serbia, in 2003, 2008, and 2014, respectively.

She is currently an Assistant Professor and the Head of the Laboratory for Biomedical Engineering and Technology, School of Electrical Engineering, University of Belgrade. She has published one book and over 60 scientific publications in the field of biomedical engineering. She has participated in four projects, with the focus on developing assistive systems for neurorehabilitation, one TEMPUS project, and one Collaborative Grant Scheme of Innovation fund of Serbia. She currently participates in the H2020 DIH-HERO Project and ITASDI Erasmus KA2+ strategic partnership project. Her research focus is on medical instrumentation design and its evaluation in clinical environment.

Dr. Janković's papers were honored with awards, including the Etran 2005 and 2014, the Telfor 2013, the Balcan congress of nuclear medicine 2015, and the Second Prize on International Medical Olympiad 2017.

ANITA V. LUP I received the B.Sc. and M.Sc. degrees in electrical engineering from the School of Electrical Engineering, University of Belgrade, Serbia, in 2017 and 2018, respectively.

She is currently pursuing the Ph.D. degree with the School of Electrical Engineering, University of Belgrade. She is currently a Junior Engineer with Novelic, Belgrade, Serbia. Her research interests include signal and image processing, robotics, and machine learning.

VELJKO R. MIHAJLOVI received the M.Sc. degree in electrical engineering from the School of Electrical Engineering, University of Belgrade, Belgrade, Serbia, in 2008.

He has been the Chief Technology Officer with Novelic, since 2013.

His current research interests are short-range mm-wave radar and its new applications in automotive, smart home, and Industry 4.0, with the special focus on people detection.

JELENA S. POPOVI -BO OVI (S'91–M'01) received the B.Sc., M.Sc., and Ph.D. degrees in electrical engineering from the School of Electrical Engineering, University of Belgrade, Serbia, in 1990, 1995, and 2000, respectively.

She is currently an Assistant Professor with the School of Electrical Engineering, University of Belgrade, Serbia. Her research interests are in the areas of integrated circuits and system design, low-power design, and relaxation oscillators.

Dr. Popović-Boović was a recipient of the Best Paper Award at TELFOR 2012, Serbia. She has served on the Technical Program Committee of the IEEE International Conference on Computer Design and TELFOR Conference. She is a reviewer of various technical journals and conferences.